Journal of Materials Chemistry C

Accepted Manuscript

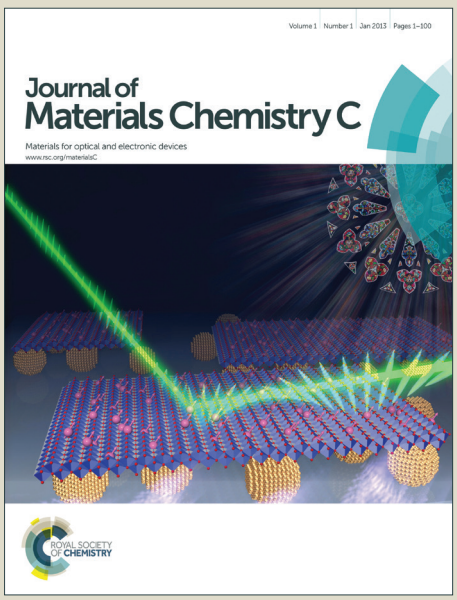

ROYAL SOCIETY OF CHEMISTRY

www.rsc.org/materialsC

Electron Spin-Polarization and Band Gap Engineering in Carbon-modified Graphitic Carbon Nitrides

Bo Yang, Hongcai Zhou, Xiaoming Zhang, Mingwen Zhao*

School of Physics and State Key Laboratory of Crystal Materials, Shandong University, Jinan 250100, Shandong, P. R. China.

E-mail: zmw@sdu.edu.cn

Abstract

Graphitic carbon nitrides are attracting increasing interests in many fields, such as fuel cells, photocatalytic decomposition of water and spintronics devices. Tailoring the electronic band gap and inducing electron spin-polarization are the keys of these applications. Using first-principles calculations, we demonstrated that these goals can be reached by modifying graphitic carbon nitride via introducing additional carbon atoms into the vacancy sites. We found that with the increase of carbon concentration, the band gap of graphitic carbon nitride decreases rapidly and comes to close as the carbon concentration is higher than 2.609%, leading to a semiconductor-metal phase transition. More interestingly, local magnetic moments appear in the triangular domain centered by the introduced carbon atom and interact in a ferromagnetic or "antiferromagnetic" way depending on their relative positions. The tunable band gap and ferromagnetism revealed in the carbon-modified graphitic carbon nitrides offer a promising way to achieve applications in hydrogen generation and spintronics devices.

1 Introduction

Graphitic carbon nitrides have been studied for more than one hundred years.[1] The interests in these two-dimensional (2D) organic materials were aroused recently owing to their potential applications in fuel cells, photocatalysis, and hydrogen production.[2-7] There are two prevailing building blocks, *s*-triazine (C_3N_3) and *tri*-*s*-triazine (C_6N_7), in the frameworks of graphitic carbon nitride materials.[8-12] These units are linked together by sp^2-hybridized nitrogen (or carbon) atoms, leading to a chemical formula of C_3N_4 (or C_4N_3),[13, 14] or directly joint together via C-C covalent bonds with a chemical formula of C_6N_6.[15] This gives rise to abundant polytypes of graphitic carbon nitrides. Theoretical works have showed that these graphitic carbon nitride materials exhibit exotic properties, such as electron spin-polarization,[16, 17] half-metallicity,[18, 19] spin-gapless semiconducting,[20, 21] and topological nontriviality.[22, 23]

The graphitic carbon nitride with a formula of C_3N_4 (denoted as g-C_3N_4) is the most stable allotrope at ambient conditions, as indicated by first-principles calculations.[24-27] Indeed, it has been synthesized successfully using different methods, such as chemical vapor deposition (CVD) method [28] and cross-linking nitride-condition anions in ionic liquid.[10] In contrast to the zero-band-gap feature of graphene, g-C_3N_4 is a semiconductor with a band gap of 2.970 eV (*s*-triazine) or 2.880 eV (*tri*-*s*-triazine).[29] The band alignment with respect to the oxidation and reduction potentials of water is suitable for hydrogen generation from water splitting. However, the band gap of g-C_3N_4 covers only the high energy bands of light. Reducing the band gap to utilize the low energy bands is the key to improve the hydrogen generation efficiency. Additionally, the ground state of g-C_3N_4 is spin-degenerated. Inducing electron spin-polarization in g-C_3N_4 is crucial for applications in spintronics.[30]

Based on first-principles calculations, we predicted that these two goals can be reached by modifying g-C_3N_4 with carbon atoms. We introduced additional carbon atoms into the porous framework of g-C_3N_4, which can be achieved by increasing the chemical potential of carbon. These carbon atoms prefer to occupy the vacancy sites

of g-C_3N_4, forming C-N covalent bonds with nearest N atoms. The band gap is sensitive to the carbon concentration and comes to close at the concentration of about 2.609%. Each dopant atom induces a local magnetic moment of 2.0 μ_B locating in the triangular domain centered by the introduced carbon atom. These magnetic moments prefer to interact ferromagnetically or antiferromagnetically, exhibiting clear anisotropy features. This work is expected to offer a promising approach to engineering the band gap and spins of g-C_3N_4.

2 Methods and computational details

We performed first-principles calculations in the framework of the density-functional theory (DFT) which is implemented in the Vienna *ab initio* simulation package known as VASP.[31, 32] The electron-ion interaction was treated by using projector-augmented-wave (PAW) potentials.[33] The exchange-correlation functional under a generalized gradient approximation (GGA) in the form proposed by Perdew, Burke and Ernzerhof (PBE) was adopted to describe the electron-electron interaction.[34] The energy cutoff employed for plane wave expansion of electron wavefunctions of both carbon and nitrogen atoms were set to 520 eV. The supercells were repeated periodically on the *x*-*y* plane while a vacuum region of about 15 Å was applied along the *z*-direction to avoid mirror interaction between adjacent images. The Brillouin zone (BZ) integration was sample on a grid of 3×3×1 k-points for structural optimizations. Structural optimizations were carried out using a conjugate gradient method until the remanent force on each atom is less than 0.01 eV/Å.

3 Results and discussion

As a benchmark, we first calculated a pristine g-C_3N_4 monolayer composing of *s*-triazine as building blocks using the above-mentioned theoretical strategy. The optimized g-C_3N_4 structure has the C-N bond lengths of 1.327Å (within a triazine ring) and 1.462 Å (between adjacent triazine rings) and lattice vectors of 4.784 Å, respectively. The electron energy band gap obtained from the PBE functional is about 1.572 eV, which is smaller than the experimental value 3.100 eV, [8] due to the

well-known failure of PBE function in predicting the band gap values of semiconductors. However, it has been widely accepted that the trend of the band gaps given by PBE functional is reasonable. These data are in good agreement with those reported in many previous theoretical works.[19]

We then moved on to the possibility of doping g-C_3N_4 with carbon atoms. We considered a large supercell of g-C_3N_4 containing 4×4 unit cells and an additional carbon atom, corresponding to a concentration of 0.885% (for additional carbon atoms). The carbon atom occupies the vacancy site surrounded by three pyridine-type nitrogen atoms. Structural optimization indicates that the carbon atom can chemically bond to the three pyridine-type nitrogen atoms with a C-N bond length of 1.354 Å. The incorporation of carbon atom induces bond relaxation nearby. The length of the C-N bond in the triazine is elongated to 1.422 Å. The changes of the bond lengths with respect to the pristine one in the proximity of the carbon atom are shown in Fig. 1(a). Clearly, the structural distortion takes place mainly around the carbon atom.

The energetically preferable distribution patterns of the carbon atoms were also considered by introducing two additional carbon atoms into a 4×4 supercell of g-C_3N_4. Due to the symmetry of the supercell, the two carbon atoms have three typical distribution patterns, as shown in Fig. 1(b)-(d), where the two additional carbon atoms are separated by different distances. Our first-principles calculations showed that the energetically most favorable pattern has the longest distance between the two carbon atoms, as shown in Fig. 1(b). This clearly indicates that at low concentration, the carbon atoms prefer to locate as far away as possible to relax the local strain. This feature has also been verified in a 3×3 supercell doped with two carbon atoms. In the following parts, we focus on this energetically preferable distribution pattern to study the electronic band structures of the carbon-modified g-C_3N_4 monolayer.

To evaluate the energetic favorability of the carbon modification, we define a formation energy (E_{form}) as $E_{form} = (E_{CN+C} - E_{CN} - n\times\mu_C,)/n$ where E_{CN+C} and E_{CN} are the total energies of g-C_3N_4 with and without the additional carbon atoms, respectively. The number of the carbon atoms incorporated into one supercell is represented by n. The chemical potential of carbon atoms μ_C is highly dependent on

the carbon resources. We therefore considered a wide range of chemical potential to reveal the dependence of formation energy on the chemical potential of carbon atom. Fig. 2 shows the variation of the formation energies of the carbon-modified g-C_3N_4 as a function of the chemical potential of carbon atom. The g-C_3N_4 modified by carbon atoms with different concentrations was considered. The highest concentration 12.5%, corresponds to the case that all the vacancy sites of the g-C_3N_4 monolayer are occupied by carbon atoms, leading to a graphene-like carbon nitride with a stoichiometry of CN. The negative formation energies of these carbon-modified g-C_3N_4 monolayers at a wide-range of chemical potentials of carbon atoms suggest their high synthetic plausibility.

We then turned to the electronic structures of these carbon-modified g-C_3N_4 monolayers. For the lowest carbon concentration considered in this work (adding one carbon into a 4×4 supercell), there is a spin-polarized ground state with a local magnetic moment of 2.0 μ_B in one supercell. The spin-resolved electronic band structures are plotted in Fig. 3(a). Spin-polarized local states with a spin-splitting of about 0.436 eV appear in the band gap of g-C_3N_4 monolayer. The electron density profiles of the wavefunctions of the flat bands are plotted in Fig. 3(b). From this figure, we can see that these electronic states are localized in the triangular domain centered by the introduced carbon atom and display the features of p_z atomic orbitals. To further reveal the origins of the spin-polarization, we plotted the orbital-resolved electron density of states (PDOS) projected onto the atoms in the triangular domain and far away from the domain as indexed in Fig. 4(a). Fig. 4(b)-4(h) give the PDOS of these atoms. It is clear that these local states arise mainly from the p_z orbital of the C_2, C_3, and N_1 atoms. The contribution of the carbon atom incorporated into the g-C_3N_4, however, is almost neglectable. This is in good consistent with the electron density profiles of the wavefunctions of the flat bands shown in Fig. 3(b). Moreover, the spin-splitting of the flat bands is about 0.436 eV, suggesting the stability of the spin-polarization. Such electron spin-polarization in triangular domains has also been found in graphene nanoflakes [35] or graphene domains embedded in BN, [36] which was attributed to the zero-energy-states of the honeycomb lattices. We also calculated the

electronic structures of an isolated $C_{12}N_{10}H_3$ triangular domain and found that it has a spin-polarized ground state with a magnetic moment of 1.0 μ_B. Although the $C_{12}N_{10}H_3$ triangular domain has more p_z electrons than in the graphene nanoflakes with the same size due to the nitrogen atoms, the origins of the electron spin-polarization are very similar.

The exchange interaction between these local magnetic moments is a quite interesting issue. We adopted two model systems with different symmetries to revel the magnetic coupling between adjacent local magnetic moments. One has two local magnetic moments in a 4×4 supercell, another contains two local magnetic moments in a 3×6 supercell, as shown in Fig. 5(a) and Fig. 5(b), which represent different alignments of the local magnetic moments. Starting from different initial spin configurations, our self-consistent calculations gave two types of magnetic orderings. One exhibits the features of ferromagnetic (FM) ordering, as shown in Fig. 5(a) and 5(b), another has the local magnetic moments aligning in an 'antiferromagnetic' (AFM) way, as indicated by the spin-polarized electron density profiles shown in Fig. 5(c). For the first model, self-consistent DFT calculations always converged to a FM state independent of initial spin configurations, suggesting that the FM ordering is energetically most preferable, as shown Fig.5 (a). The second model, however, showed that the AFM ordering is slightly more stable than the FM ordering by about 0.016 eV. This implies that the exchange interaction between these local magnetic moments is highly dependent on their relative positions, exhibiting clear anisotropy features. Anyway, modifying g-C_3N_4 with carbon atoms is an efficient way to induce electron spin-polarization, which is essential for applications in spintronics.

It is noteworthy that with the increase of carbon concentration, for example, modifying g-C_3N_4 by adding one carbon atom into a 3×3 supercell, one of the flat bands becomes dispersive in the reciprocal space, as shown in Fig. 6(a). The overlap of the electron wavefunctions between adjacent triangular domains leads to delocalization of the electronic states, resulting in dispersive bands. This narrows the band gap of g-C_3N_4. We can reasonably deduce that with the increase of carbon concentration the band gap of g-C_3N_4 may close, giving rise to a

semiconductor-to-metal phase transition. We calculated the electronic band structures of g-C_3N_4 modified by different numbers of carbon atoms. It was found that the band gap was indeed closed as the carbon concentration exceeds 2.609%, as shown in Fig. 6(b). For the highest carbon concentration, *i.e.*, all the vacancies of g-C_3N_4 are occupied by carbon atoms, the resulted g-CN is metallic without electron spin-polarization, as shown in Fig. 6(c). The electron spin-polarized is quenched in this case due to the delocalized electronic states. The band gap of the carbon-modified g-C_3N_4 decreases rapidly with the increase of carbon concentration and comes to close as the carbon concentration exceeds 2.609%, as shown in Fig. 6(d). The critical carbon concentration corresponds to doping a 4×4 supercell with three carbon atoms. There are numbers of doping configurations at this concentration, and some of them are semiconducting. However, the metallic configuration shown in the insets of Fig. 6(d) is energetically most favorable. Engineering the electronic band gap of g-C_3N_4 to meet the requirement of photocatalysis and hydrogen production is quite crucial for practice applications. The sensitivity of the electronic band structures of g-C_3N_4 in response to carbon modification offers a promising way to reach this goal.

It is noteworthy that foreign atoms can also be incorporated to the frameworks of g-C3N4 by substituting the nitrogen atoms.[30,37,38] The electron spin-polarization[30] and tunable band gaps [37,38] of these carbon-doped g-C_3N_4 have also been proposed. Compared with the substitutional patterns, incorporating carbon atoms into the vacancies of g-C_3N_4 can largely recover the π conjugation of honeycomb lattices and reduce the band gap efficiently. Additionally, the synthetic routes of these two patterns would be quite different. Although, the g-C_4N_3 formed by substituting the three-coordinated nitrogen atoms of g-C_3N_4 with carbon atoms [18] is energetically more favorable than the g-CN (with all the vacancies of g-C_3N_4 been fully occupied by carbon atoms) by about 0.88 eV/atom under carbon-rich conditions, high synthetic plausibility of incorporating carbon atoms into the vacancies of g-C_3N_4 could be expected, because it is almost barrierless as atomic carbon resources are supplied.

4 Conclusions

Using first-principles calculations, we predicted that the electronic properties of g-C_3N_4 can be well-tuned by incorporating carbon atoms into the vacancies of the framework. The carbon atoms prefer to locate with the separation as far as possible to relax the strain. The formation energy calculations showed that carbon modification has high plausibility in a wide range of the chemical potential of carbon atoms. At low concentration, the incorporated carbon atoms can induce spin-polarized local states in the band gap of g-C_3N_4. The local magnetic moments arising from these local states interact in a ferromagnetic or "antiferromagnetic" way depending on their relative positions, exhibiting clear anisotropy features. The band gap of the carbon-modified g-C_3N_4 decreases rapidly with the increase of carbon concentration and comes to close as the concentration exceeds 2.609%. The sensitivity of the electronic band structures of g-C_3N_4 in response to carbon modification provides a promising way to tune the electronic properties of g-C_3N_4 to fulfill the requirements of wide-range applications, such as photocatalysis, hydrogen production, and spintronics devices.

Acknowledgments

This work is supported by the National Basic Research Program of China (No. 2012CB932302), the National Natural Science Foundation of China (Nos. 91221101, 21433006), the 111 project (No. B13029), the Taishan Scholar Program of Shandong, and the National Super Computing Centre in Jinan.

References

1 E. C. Franklin, *J. Am.Chem. Soc*, 1922, **44**, 486-509.
2 X. Wang, S. Blechert and M. Antoniett, *ACS Catal.*, 2012, **2**, 1596-1606.
3 L. Ge, F. Zuo, J. Liu, Q. Ma, C. Wang, D. Sun, L. Bartels and P. Feng, *J. Phys. Chem. C*, 2012, **116**, 13708-13714.
4 Y. Zheng, J. Liu, J. Liang, M. Jaroniec and S. Z. Qiao, *Energy Environ. Sci.*, 2012, **5**, 6717-6731.
5 F. Wu, Y. Liu, G. Yu, D. Shen, Y. Wang and E. Kan, *J. Phys. Chem. Lett.*, 2012, **3**, 3330-3334.
6 Q. Xiang, J. Yu and M. Jaroniec, *J. Phys. Chem. C*, 2011, **115**, 7355-7363.

7 Y. Wang, X. Wang and M. Antonietti, *Angew. Chem*, 2012, **51**, 68-89.

8 V. N. Khabashesku, J. L. Zimmerman and J. L. Margrave, *Chem. Mater.*, 2000, **12**, 3264-3270.

9 A. Thomas, A. Fischer, F. Goettmann, M. Antonietti, J. O. Müller, R. Schlögl and J. M. Carlsson, *J. Mater. Chem.*, 2008, **18**, 4893-4908.

10 E. Kroke, M. Schwarz, E. Horath-Bordon, P. Kroll, B. Noll and A. D. Norman, *New J. Chem.*, 2002, **26**, 508-512.

11 B. Jürgens, E. Irran, J. Senker, P. Kroll, H. Müller and W. Schnick, *J. Am. Chem. Soc.*, 2003, **125**, 10288-10300

12 J. Sehnert, K. Baerwinkel and J. Senker, *J. Phys. Chem. B*, 2007, **111**, 10671-10680.

13 J. S. Lee, X. Wang, H. Luo and S. Dai, *Adv. Mater.*, 2010, **22**, 1004-1007.

14 M. Groenewolt and M. Antonietti, *Adv. Mater.*, 2005, **17**, 1789-1792.

15 J. Li, C. Cao, J. Hao, H. Qiu, Y. Xu and H. Zhu, *Diam. Relat. Mater.,*2006, **15**, 1593-1600.

16 D. Ghosh, G. Periyasamy and S. K. Pati, *J. Phys. Chem. C*, 2014, **118**, 15487-15494.

17 H. Pan, H. Zhang, H. Liu and L. Chen, *Solid State Commun*, 2015, **203**, 35-40.

18 A. Du, S. Sanvito and S. C. Smith, *Phys. Rev. Lett.*, 2012, **108,** 197207.

19 J. Zhang, X. Gong, B. Xu, Y. Xia, J. Yin and Z. Liu, *Phys. Status Solidi B*, 2014, **251**, 1386-1392.

20 Y. Li, Z. Zhou, P. Shen and Z. Chen, *ACS Nano*, 2009, **3**, 1952-1958.

21 X. Zhang, A. Wang and M. Zhao, *Carbon*, 2015, **84**, 1-8.

22 X. Zhang and M. Zhao, *RSC Adv.*, 2015, **5**, 9875-9880.

23 A. Wang, X. Zhang and M. Zhao, *Nanoscale*, 2014, **6**, 11157-11162.

24 D. M. Teter and R. J. Hemley, *Science*, 1996, **271**, 53-55.

25 A. Y. Liu and R. M. Wentzcovitch, *Phys. Rev. B: Condens. Matter Mater. Phys.*, 1994, **50**, 10362-10365.

26 J. E. Lowther, *Phys. Rev. B: Condens. Matter Mater. Phys.*, 1999, **59**, 11683-11686.

27 J. Ortega and O. F. Sankey, *Phys. Rev. B: Condens. Matter Mater. Phys.*, 1995, **51**, 2624-2627.

28 J. Kouvetakis, A. Bandari, M. Todd and B. Wilkens, *Chem. Mater.*, 1994, **6**, 811-814.

29 Y. Xu and S. P. Gao, *Int. J. Hydrogen Energy*, 2012, **37**, 11072-11080.

30 X. Zhang, M. Zhao, A. Wang, X. Wang and A. Du, *J. Mater. Chem. C.*, 2013, **1**. 6265-6270.

31 G. Kresse and J. Hafner, *Phys. Rev. B: Condens. Matter Mater. Phys.*, 1993, **48**, 13115-13118.

32 G. Kresse and J. Furthmüller, Phys. Rev. B: Condens. Matter Mater. Phys., 1996, **54**, 11169-11186.

33 G. Kresse and D. Joubert, *Phys. Rev. B: Condens. Matter Mater. Phys.*, 1999, **59**, 1758-1775.

34 J. P. Perdew, K. Burke and M. Ernzerhof, *Phys. Rev. Lett.*, 1996, **77**, 3865-3868.

35 J. Fernández-Rossier1 and J. J. Palacios, *Phys. Rev. Lett.*, 2007, 99, 177204

36 A. Wang, M. Zhao, Y. Xi, X. Wang and Z. Wang, *Phys. Lett. A*, 2013, **377**, 1102-1103

37 G. Dong, K. Zhao and L. Zhang, *Chem. Commun.*, 2012, **48**, 6178-6180

38 X. Ma, Y. Lv, J. Xu, Y. Liu, R. Zhang and Y. Zhu, *J. Phys. Chem. C*, 2012, **116**,

23485-23493

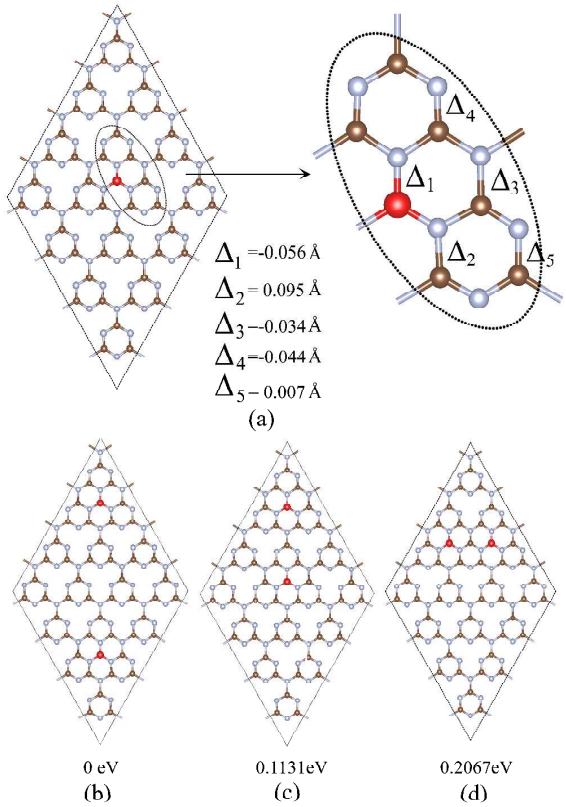

Figure 1 (a) Schematic representation of the atomic structure of carbon-modified g-C_3N_4 with an additional carbon atom (red ball) in a 4×4 supercell. The bond relaxation in the vicinity of the incorporated carbon atom is indicated in the right panel. The numbers represent the changes of the bond length with respect to pristine g-C_3N_4. (b), (c) and (d) were the configurations of the g-C_3N_4 with two additional carbon atoms (red ball) in a 4×4 supercell. The numbers are the energies relative to the energetically most favorable configurations. Carbon and nitrogen atoms in g-C_3N_4 are indicated by the brown and light balls, respectively.

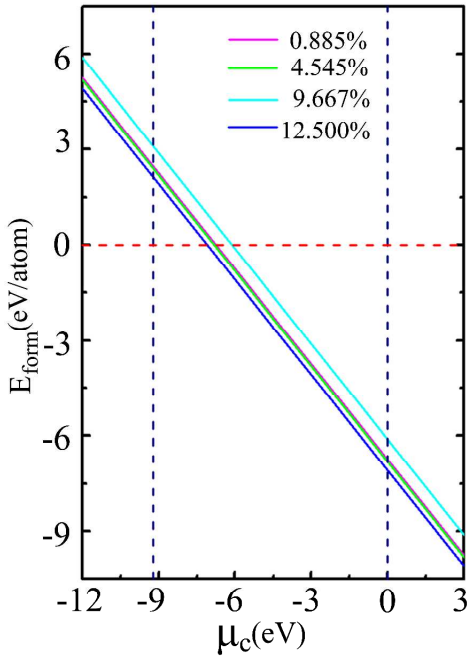

Figure 2 Formation energies of carbon-modified g-C_3N_4 with different carbon concentrations vary as a function of the chemical potential of carbon (μ_C). The chemical potential of a free carbon atom was set to zero. The chemical potential of carbon in graphene is indicated by the dashed line.

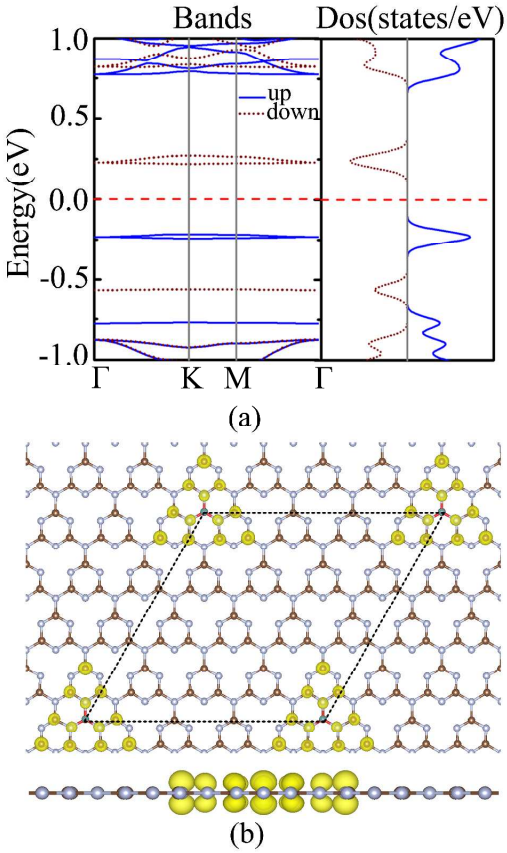

Figure 3 (a) The spin-resolved electronic band structure of the carbon-modified g-C_3N_4 with one additional carbon atom in a 4×4 supercell. The energy at the Fermi level was set to zero. (b) The electron density profiles of the wavefunctions of the flat bands nearest to the Fermi level.

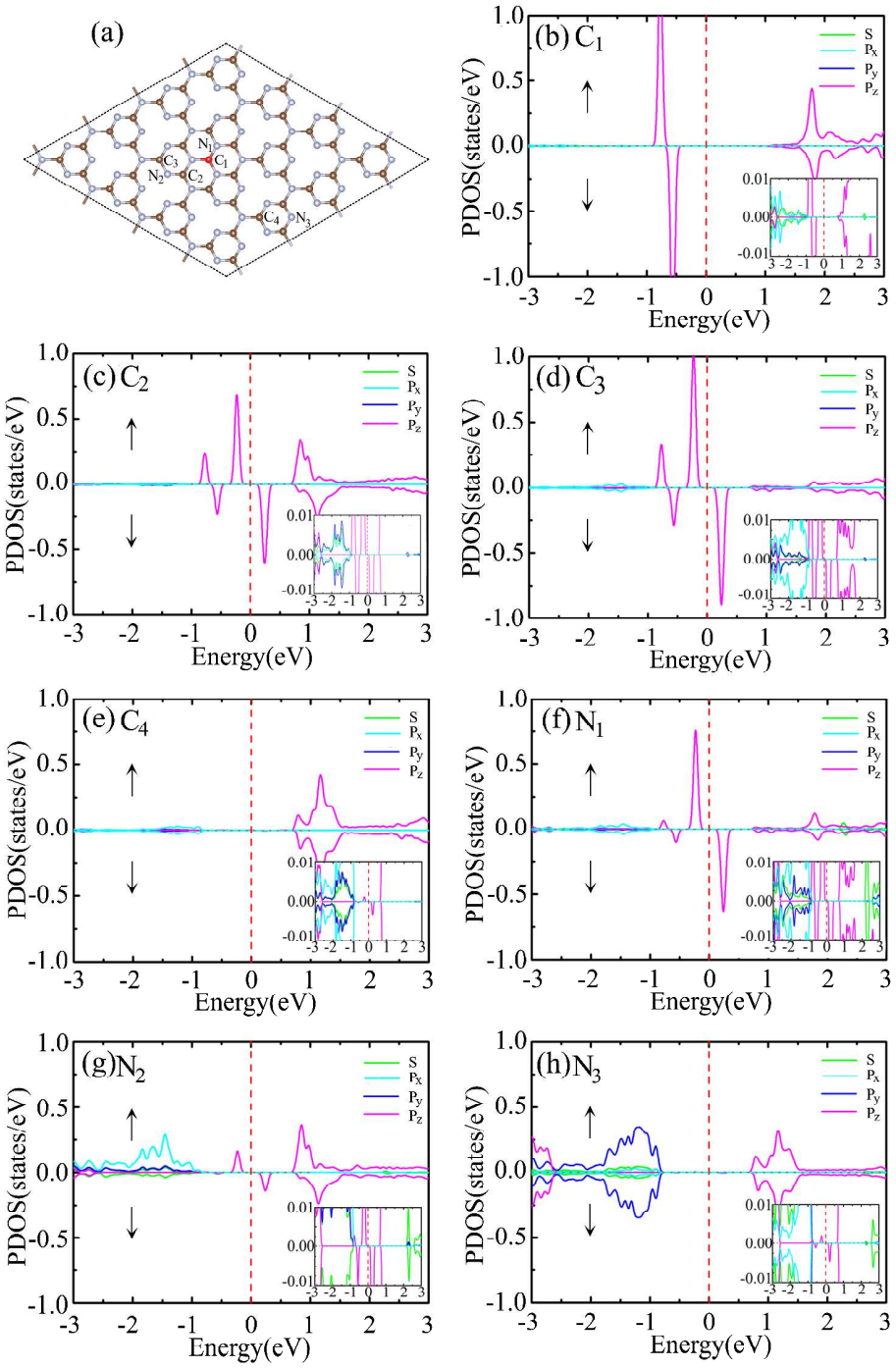

Figure 4 The orbital-resolved electron density of states (PDOS) projected on to the different atoms indexed in (a). The up and down panels in each figure indicate the contribution of spin-up and spin-down branches. The enlarged views of the PDOS near the Fermi level are plotted in the insets of this figure. The energy at the Fermi level was set to zero.

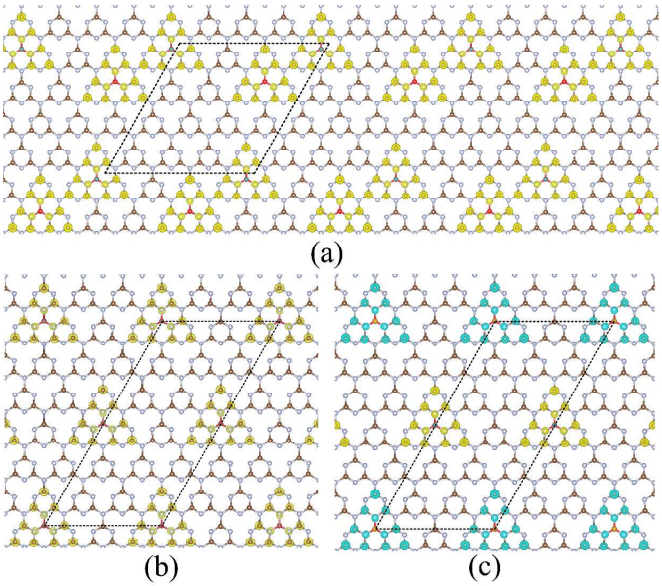

Figure 5 Spin-polarized electron density profiles of carbon-modified g-C_3N_4 with two additional carbon atoms in one supercell. (a) The FM ordering in a 4×4 supercell. (b) FM and (c) AFM orderings in a 3×6 supercell. Spin-up and spin-down components are indicated by yellow and blue bubbles, respectively.

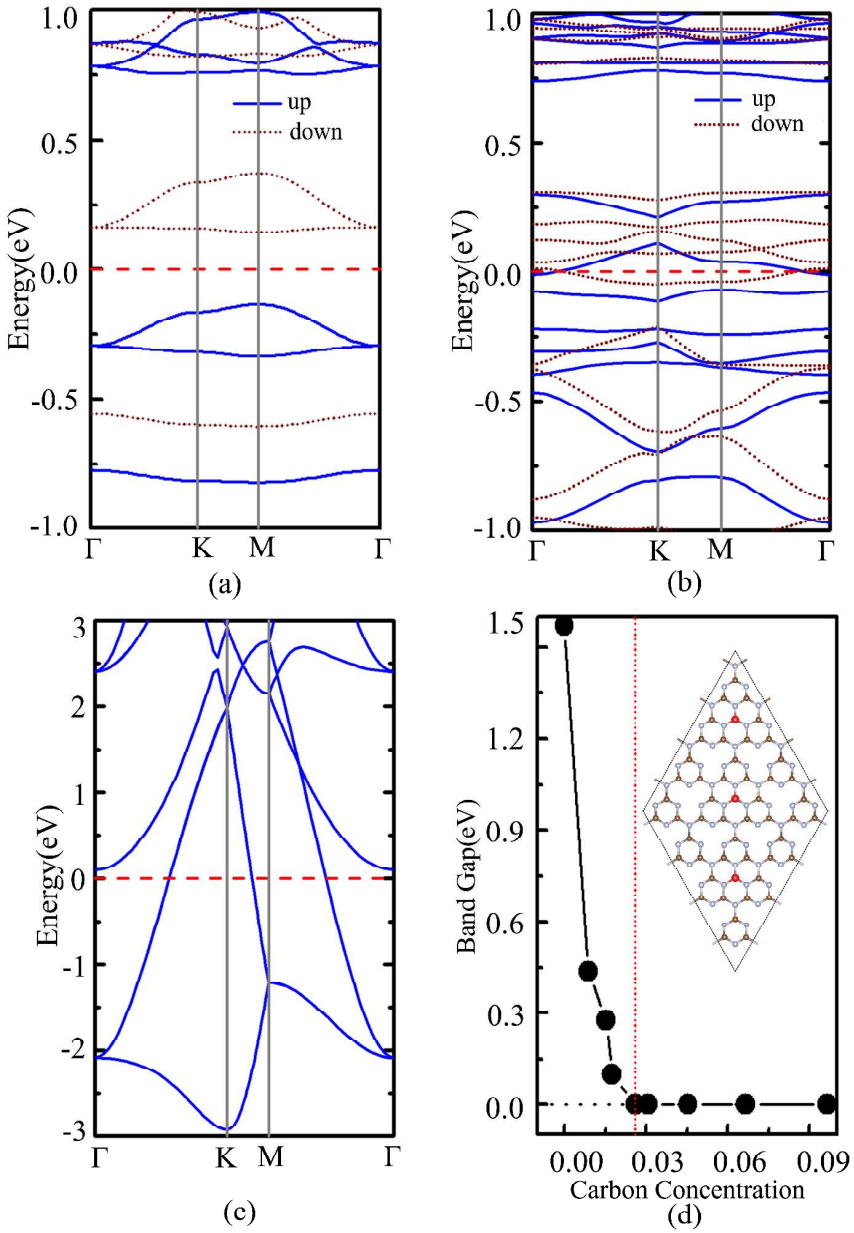

Figure 6 (a)-(c) Electron band structures of carbon-modified g-C_3N_4 with the carbon concentrations of 1.526%, 2.609%, and 12.5%. The energy at the Fermi level was set to zero. (d) Energy band gaps of the carbon-modified g-C_3N_4 with different carbon concentrations. The configuration corresponding to the critical carbon concentration, 2.609% is shown in the insets of (d). Three additional carbon atoms are indicated by the red balls.

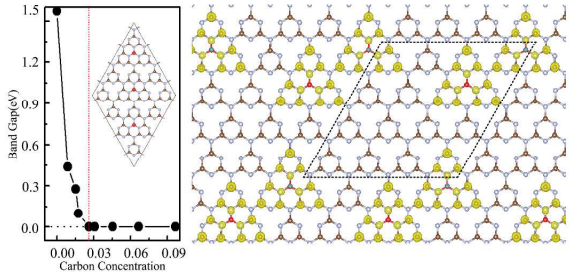

Carbon doping induces a semiconductor-metal phase transition in g-C_3N_4 with the rapid decrease of band gap and spin-polarization.